Polymer 90 (2016) 18–25

Contents lists available at ScienceDirect

Polymer

journal homepage: www.elsevier.com/locate/polymer

Interfacial crystallization and mechanical property of isotactic polypropylene based single-polymer composites

Liying Zhang [a], Yijing Qin [a], Guoqiang Zheng [a, ***], Kun Dai [a], Chuntai Liu [a], Xingru Yan [b], Jiang Guo [b], Changyu Shen [a, **], Zhanhu Guo [b, *]

[a] College of Materials Science and Engineering, The Key Laboratory of Material Processing and Mold of Ministry of Education, Zhengzhou University, Zhengzhou, 450001, PR China
[b] Integrated Composites Laboratory (ICL), Department of Chemical & Biomolecular Engineering, University of Tennessee, Knoxville, TN 37996, USA

ARTICLE INFO

Article history:
Received 14 December 2015
Received in revised form
14 February 2016
Accepted 21 February 2016
Available online 23 February 2016

Keywords:
Single-polypropylene composites
Transcrystallinity
Tensile strength

ABSTRACT

Isotactic polypropylene (iPP) based single-polymer composites (SPCs) were prepared by introducing iPP fibers into the molten or supercooled homogeneous iPP matrix. The influences of fiber introduction temperature (T_i) on the resultant morphology of transcrystallinity (TC) and mechanical properties of SPCs were investigated via a polarized optical microscopy (POM) and a universal tensile test machine. The effects of interfacial crystallization on mechanical properties were also studied. The tensile strength of SPCs was observed to increase firstly and to reach a maximum value at $T_i = 160$ °C, and then to decrease with further increasing the T_i. Wide-angle X-ray diffraction (WAXD), scanning electron microscopy (SEM) and POM were employed to understand the mechanical enhancement mechanism. It is found that the enhanced tensile strength of SPCs was strongly dependent on the synergistic effects of TC, high orientation degree of iPP fibers and good adhesion between the iPP fiber and the matrix.

1. Introduction

In the past few decades, isotactic polypropylene (iPP) has been the major polymeric construction materials in the light of its impressive consumption. One outstanding advantage is its excellent comprehensive properties, including easy processing, low manufacturing cost and so on [1]. Unfortunately, the intrinsic low mechanical strength of iPP limits its further applications. Hence, considerable efforts have been made in order to further improve its mechanical properties. One of the most common methods is by embedding various fibers (carbon, clays, glass, etc.) in the iPP matrix to produce composites [2–5]. However, two main problems must be avoided if the heterogeneous fibers are added in the thermoplastic matrix. The first is the interfacial residual stress due to different thermal expansion between heterogeneous fibers and polymer matrix [4]. The second is the weak interfacial adhesion owing to the incompatibility among the heterogeneous components [6]. The interfacial interaction between fiber and matrix is a crucial prerequisite for determining the mechanical property [7]. Among the various methods (including the increased specific surface area of fibers, improved chemical activity of fiber surfaces, and matched compatibility) to enhance the interfacial interaction in the iPP/fibers composites [8–14], interfacial crystallization such as transcrystallinity (TC) [15] is regarded as an efficient and economical approach [16]. Moreover, TC around the fiber, possessing better load transfer ability than amorphous layers, is believed to be of crucial significance to improve the interfacial interaction between matrix and fibers [17,18].

On the other hand, in light of recyclability, the presence of heterogeneous additives or inclusions, such as glass fibers, clays and magnetic nanoparticles, is an inevitable obstacle for polymer based composites. Hence, the composite systems with the matrix and the fiber being from the same polymer are preferable candidates. In other words, these systems mean mono-component composites or single-polymer composites (SPCs). The concept of SPCs is not new, which was proposed for the first time by Capiati and Porter four decades ago [19]. Such self-reinforced systems have specific economic and ecological advantages. This can be understood as follows: 1) desired mechanical property can be achieved as a result of the occurrence of TC and good interfacial adhesion for

* Corresponding author.
** Corresponding author.
*** Corresponding author.
E-mail addresses: gqzheng@zzu.edu.cn (G. Zheng), shency@zzu.edu.cn (C. Shen), zguo10@utk.edu (Z. Guo).

http://dx.doi.org/10.1016/j.polymer.2016.02.052
0032-3861/

the semicrystalline polymer matrix; 2) SPCs show undoubtedly advantages in terms of recyclability. Hence, up to now, many preparation methods of iPP based SPCs have been proposed [20–22] and summarized in the recent literature [23–25]. However, although the influences of crystallization temperature, fiber introduction temperature, fiber molecular weight, and matrix molecular mass on the interfacial morphology of iPP based SPCs have been investigated [26–29], the effect of interfacial features on the mechanical properties of SPCs has been rarely reported up to date.

In this paper, iPP fiber was introduced into iPP film to prepare iPP based SPCs. The interfacial features of SPCs and their tensile strength as a function of introduction temperature were investigated. The underlying origin for the improved tensile strength of SPCs is discussed based on the results of polarized optical microscopy (POM), scanning electron microscope (SEM), wide-angle X-ray diffraction (WAXD).

2. Experimental

2.1. Materials

The iPP (T30S) employed in this work was a commercial grade iPP, provided by Dushanzi Petroleum Chemical Co. Ltd, China. Its melt flow index (*MFI*) and weight-average molecular weight (M_w) were 3.0 g/10 min (230 °C, 21.6 N) and 39.93 × 10^4 g/mol, respectively.

2.2. Melt spinning

The iPP fibers used in this work were melt spun by using a mini co-rotating twin-screw extruder (SJSZ-10A, Wuhan Ruiming plastic and mechanical Co. Ltd) with a length-to-diameter ratio (L/D) of 16 and a die diameter of 3.0 mm. The temperature of both barrel and die was 200 °C. The spun fibers were air-cooled and taken up by a winder. To obtain the finest fibers, the screw speed and the take-up speed were maintained at 1 rpm and 30 m/min, respectively. In the case of the highest take-up speed, it produces a fiber with a draw ratio (area of extruder die vs. section area of iPP fiber) of 100. The average diameter of the as-prepared iPP fibers was ca. 30 um. The iPP fibers were first rinsed several times in acetone with the aid of ultrasonication, then cleaned with deionized water, and finally dried in a vacuum oven at 40 °C for 5 h. The melting behaviors of iPP fibers and granules were obtained by differential scanning calorimeter (DSC) method, which are shown in Fig. S1 in Supplementary data. Compared with iPP granules, iPP fibers have a higher melting point, which provides a prerequisite for the SPCs preparation. At the same time, molecular orientation, crystal modification and tensile strength of iPP fiber were also investigated, which are shown in Fig. S2, S3 and S4 in Supplementary data.

2.3. SPCs preparation

Firstly, iPP thin film as matrix was prepared by compression-molding at 200 °C with a pressure of 10 MPa. The resultant iPP thin film was subsequently heated in a well-controlled hot stage (Linkam, THMS600) at 200 °C and maintained for 10 min to remove any possible thermal history effects. Then, the iPP thin film was cooled at a rate of 30 °C/min to the preset temperature (viz., introduction temperature, T_i), where the film was maintained in the molten or supercooled molten state. Once the molten or supercooled molten iPP thin film reached an equilibrium at T_i, the iPP fiber supported by a metal frame was introduced into the film (iPP matrix). Subsequently, the sample was cooled quickly to the isothermal crystallization temperature (T_c, 134 °C) at a rate of 30 °C/min, at which the isothermal crystallization of SPCs was allowed for 10 min. The iPP fiber quality content, viz., volume content (C) of SPC is calculated as 0.59% (C was estimated as the fractional area occupied by iPP fiber in the entire tensile sample). The thermal history of SPCs preparation was shown in Fig. 1. For comparison, the pure iPP film without fiber introduction was also prepared with the same thermal history as that of SPCs. According to the melting behavior of iPP fibers (shown by Fig. S1 in Supplementary data), the iPP fiber introduction temperature (T_i) used in this study was selected as 145, 160, 165, 168, 172, and 175 °C, respectively. In a convenient manner, the SPCs prepared at different T_i were labeled as SPC-X and the iPP fibers experienced the same thermal history as that of SPCs were labeled as F-X, where X represents T_i. For example, "SPC-145" denotes a sample prepared at $T_i = 145$ °C, while "F-145" denotes the fiber experienced the same thermal history as that in SPC-145.

2.4. Characterizations

Polarized Fourier Transform Infrared Spectroscopy (FTIR) spectrometer equipped with a hot stage (Linkam, THMS600) under a flowing nitrogen atmosphere was employed to analyze the relationship between molecular orientation and T_i. Before measurements, the iPP fiber was tightly fixed on a metal frame between two parallel ZnSe plates. The iPP fiber was first heated to T_i and held for 2 min, then cooled quickly to T_c (134 °C) at a rate of 30 °C/min. At 134 °C, the isothermal crystallization of iPP fiber was also allowed for 10 min. Finally, the molecular orientation of iPP fiber was qualitatively investigated by the FTIR equipped with a polarizer (NICOLET 6700). The resolution was set as 2 cm^{-1} with an accumulation of 32 scans. The scanned wavenumber range was from 400 to 4000 cm^{-1}.

Tensile strength of SPCs was determined by a universal tensile test machine (UTM2203, Shenzhen Suns Technology Stock Co., Ltd, China) with a load cell of 100 N and under a crosshead speed of 0.5 mm/min at room temperature. The mean and standard deviation were reported based on at least ten samples. Before test, the samples after isothermal crystallization were quenched immediately into a mixed ice/water solution to preserve the crystalline morphology. The SPCs were cut into rectangular geometry (10 × 2 × 0.06 mm^3) for mechanical test.

To observe the interfacial crystallization of SPCs, an Olympus BX51 POM equipped with a hot stage (Linkam, THMS600) was used in this study. The pictures were taken automatically to record the evolution of interfacial morphology at a regular time interval. Furthermore, the morphology of tensile fractured zone of SPCs was also observed by POM.

To characterize the crystalline structure of SPCs, two-

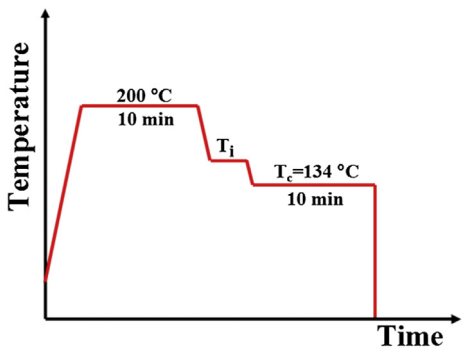

Fig. 1. Schematic of thermal history as a function of time. T_i represents the iPP fiber introduction temperature (i.e.,145, 160, 165, 168, 172, and 175 °C).

dimensional wide-angle X-ray diffraction (2D-WAXD) measurements were carried out at the beam line BL16B1 in Shanghai Synchrotron Radiation Facility (SSRF). A MAR 165 CCD detector (2048 × 2048 pixel with pixel size 80 μm) was used to collect all the 2D-WAXD images, the distance from which to sample was 118 mm. The wavelength was 0.124 nm. To achieve maximum scattering intensity, the SPCs were stacked orderly to obtain a mat with a total thickness of about 1 mm.

SEM (JEOL JSM 7500F) was employed to further investigate the crystalline morphology and interfacial adhesion between iPP fiber and matrix. Before observation, the samples were etched by the solution of potassium permanganate in a mixture of nitric acid and sulfuric acid according to the reported procedures [30] and sputtered with gold for better imaging.

3. Results and discussion

3.1. Influence of introduction temperature on molecular orientation of iPP fibers

The absorbance intensity difference between the parallel- and perpendicular-polarized FTIR spectra can be employed to evaluate the molecular orientation level [31,32]. Here, to qualitatively evaluate the effect of different thermal history on the orientation level of iPP fibers, polarized FTIR test was carried out. Fig. 2 shows the polarized FTIR spectra of F-145, F-160, F-165, F-168, F-172 and F-175, respectively. It is clear to find notable difference between the absorbance intensities of the parallel-polarized FTIR spectra and those of the perpendicular-polarized FTIR spectra, suggesting that the molecular chains are principally oriented along the fiber axis for all iPP fibers. However, the difference of absorbance intensities between the parallel- and perpendicular-polarized FTIR spectra is observed to be attenuated gradually with increasing T_i. Additionally, in order to further evaluate the extent of orientation level of iPP fiber, dichroic ratio (R) was calculated from Equation (1) [33]:

$$R = \frac{A_{\parallel}}{A_{\perp}} \tag{1}$$

where $A_{\parallel}$ and $A_{\perp}$ are the measured absorbance values for radiation polarized parallel and perpendicular to the fiber axis, respectively. Calculated R is summarized in Table 1. If the value of R is equal to 1, there is no orientation. While for an oriented sample, the value of R diverges from 1. Moreover, the greater the value of R diverges from 1, the higher the degree of orientation is. As shown in Table 1, R of all the iPP fibers diverges from 1 obviously. Furthermore, the value of R deviating from 1 becomes smaller and smaller with the increase of theT_i, indicating that the extent of orientation level of the iPP fiber indeed was attenuated with increasing T_i.

3.2. Influence of introduction temperature on interfacial morphology of SPCs

To investigate the influence of introduction temperature on the interfacial morphology of SPCs, a series of optical micrographs of the SPCs were taken during isothermal crystallization at 134 °C (see Fig. 3). On the whole, iPP crystals can be induced at the surface of iPP fiber within 1 min (shown by the arrow in Fig. 3). These crystals are so dense that they have to grow normal to the iPP fiber axis. Such resultant supermolecular structure of cylindrical symmetry is TC [15]. In other words, these dense crystals indicate that the homogeneous iPP fiber is helpful to induce crystallization of iPP matrix, which has been explained in the literature [34]. When the crystallization time approaches 2 min, spherulites in the matrix away from the iPP fiber are also observed. For SPCs prepared at lower temperatures (e.g., 145, 160, 165, and 168 °C), it is easy to distinguish the outline of iPP fiber in SPCs (see Fig. 3a–d). Unfortunately, there is no obvious change in the macroscopic level for the interfacial crystallization with the increase of T_i. With respect to SPC-172 (see Fig. 3e), the boundary between fiber and matrix is too fuzzy to be distinguished, suggesting that the iPP fiber has been partially molten. When T_i is further elevated to 175 °C (see Fig. 3f), though the boundary between fiber and matrix is absolutely disappeared because of the melting of iPP fiber (confirmed by DSC result shown in Fig. S1 in Supplementary data), it still remains active for initiating the oriented crystallization of the iPP matrix. Meanwhile, as seen from the optical micrographs of the SPCs, both TC and spherulites can be estimated as the same crystal form according to the sign of birefringence.

To investigate the crystallization kinetics of TC of SPCs prepared at different T_i, the total diameter (D_1) of TC (including iPP fiber) and the diameter (D_2) of spherulites at 20-s intervals were measured with the assistance of Image-Pro Plus software. At the same time, the diameter (D_0) of iPP fiber was also measured at the beginning of crystallization. Then the thickness (H) of TC and the radius (R) of spherulites were calculated using the following Equation (2) and (3),

$$H = (D_1 - D_0)/2 \tag{2}$$

$$R = D_2/2 \tag{3}$$

Fig. 4 shows the calculated thickness of TC and the radius of spherulites as a function of crystallization time. A linear fitting of the points (thickness or radii versus crystallization time) was done to obtain the slope, which can be considered as the growth rate [35]. It is clearly seen that there is no difference between the growth rate of TC and spherulites. This further verifies the result of POM. In other words, they are of the same crystal form.

3.3. Mechanical property

3.3.1. Tensile test of the SPCs

One of our main concerns is to reveal the relationship between interfacial features and mechanical property of SPCs prepared at different T_i. As shown in Fig. 5, tensile strength of pure iPP films generally keeps a constant value around 7.3 MPa over the entire range. For SPCs, when T_i is increased from 145 to 160 °C, the tensile strength is enhanced from 7.38 to 8.89 MPa, exhibiting an increasing amplitude of around 20.6%. However, with a further increase of T_i (from 165 to 175 °C), the tensile strength shows a decreasing trend. On the whole, except for SPC-145, the tensile strength of SPCs is steadily higher than that of pure iPP films. According to the POM results shown in Fig. 3, the spherulites in the matrix of all samples are so rare that their contribution to the mechanical property can be ignored. Therefore, the key factor for enhancing the tensile strength of SPCs must be associated with the introduction of iPP fibers, which will be discussed in detail in the following section.

3.3.2. 2D-WAXD measurements of SPCs

2D-WAXD measurements were carried out to investigate the crystalline structure of SPCs prepared at different T_i. All the 2D-WAXD patterns consist of the diffraction circles or arcs from inner to outer associated with different lattice planes of iPP (see Fig. 6), which respectively correspond to (110), (040), (130), (111) and (−131). These lattice planes originate from the α-form monoclinic packing of PP [36,37], indicating that both TC and spherulites are α-form [38]. Moreover, the 1D-WAXD curves are obtained from the circularly integrated intensities of 2D-WAXD patterns, which are

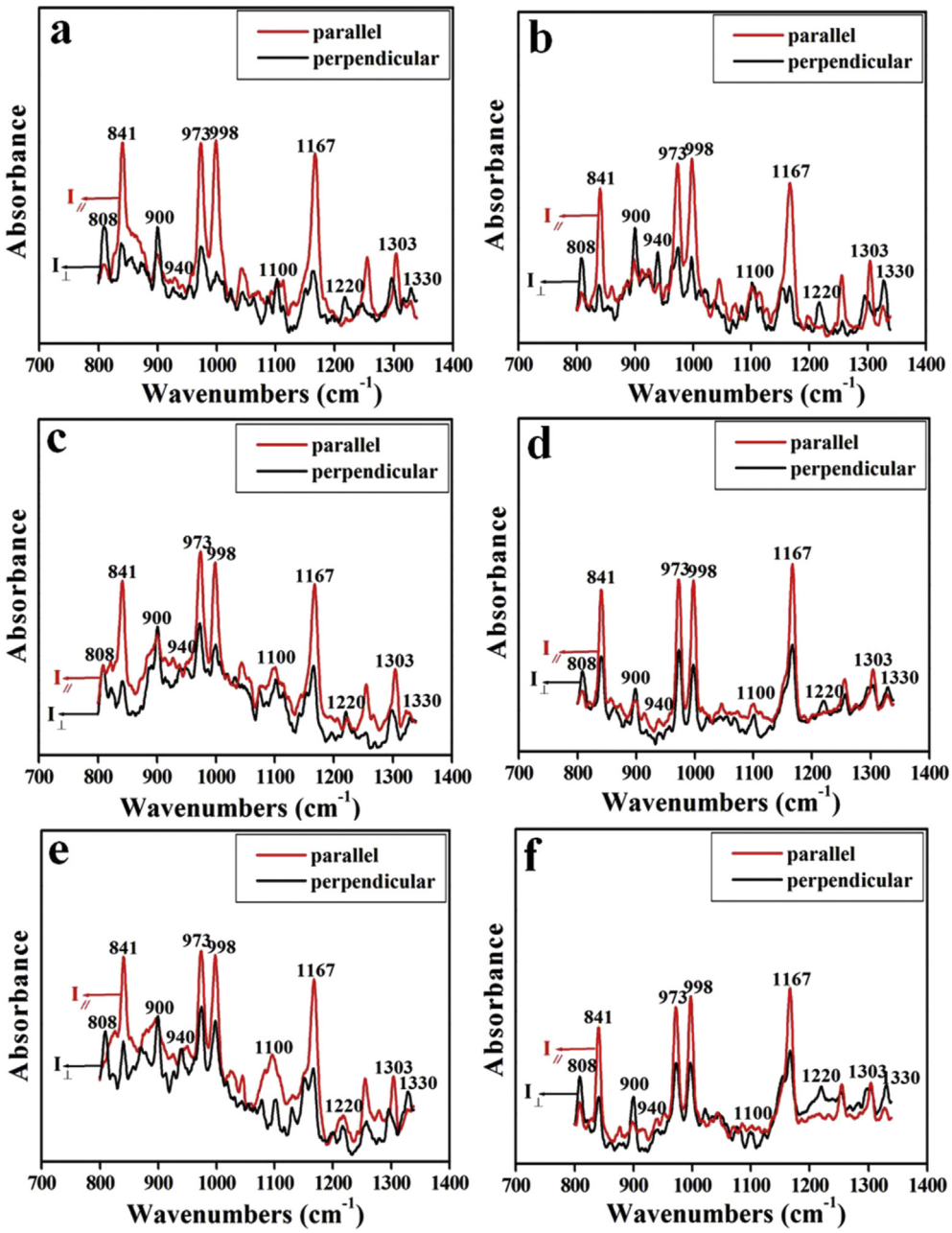

Fig. 2. Polarized FTIR spectra of iPP fibers experienced different thermal history. T_i was (a) 145, (b) 160, (c) 165, (d) 168, (e) 172, and (f) 175 °C. The red line was obtained with the infrared beam polarized parallel to the fiber axis and the black one was obtained with the infrared beam polarized perpendicular to the fiber axis (For interpretation of the references to colour in this figure legend, the reader is referred to the web version of this article.).

shown in Fig. 7. Through deconvoluting the peaks of one-dimensional wide-angle X-ray diffraction (1D-WAXD) curves, X_c can be calculated by the following equation (4) [39]:

$$X_c = \frac{\sum A_{crystal}}{\sum A_{crystal} + \sum A_{amorph}} \times 100\% \quad (4)$$

where A_{amorph} and $A_{crystal}$ are the fitted areas contributed by the amorphous and crystalline phases, respectively. According to above equation, the calculated X_c of SPCs is listed in Table 2. The X_c of SPCs has no obvious change, that is, the difference between its maximum and minimum value is less than 9%. Therefore, the effect of X_c on tensile strength can be excluded.

3.3.3. *Influence of interfacial features on mechanical property*

The mechanical property of the fibers reinforced polymer composites is substantially related to the fiber/polymer interfacial features [14,40–42]. Taking these into account, different interfacial features of the SPCs prepared at different T_i were studied. Here, according to the change trend of the tensile strength shown in Fig. 5 (that is, with the increase of the T_i, the tensile strength of SPCs firstly increases and reaches a maximum value at $T_i = 160$ °C, then decreases monotonously to the minimum value at $T_i = 175$ °C), SPC-145, SPC-160 and SPC-175 were therefore selected as representative samples to investigate the relationship between interfacial features and mechanical property. The SEM pictures are presented in Fig. 8a–c. With respect to SPC-145, SPC-160 and SPC-175, the

Table 1
Dichroic ratio of different bands of iPP fibers experienced different thermal history.

Wavenumber (cm^{-1})	Dichroic ratio (R)					
	F-145	F-160	F-165	F-168	F-172	F-175
808	0.16	0.28	0.41	0.40	0.42	0.44
841	6.68	6.10	5.41	4.92	4.09	3.13
900	0.24	0.36	0.41	0.48	0.56	0.62
940	0.43	0.48	0.53	0.66	0.72	0.73
973	2.79	2.56	2.50	2.34	2.07	2.05
998	11.64	7.11	6.18	5.43	4.97	4.81
1100	0.50	0.55	0.56	0.75	0.85	0.88
1167	2.21	2.05	1.53	1.46	1.36	1.17
1220	0.11	0.19	0.29	0.33	0.44	0.53
1303	1.90	1.76	1.6	1.57	1.46	1.26
1330	0.21	0.35	0.57	0.66	0.69	0.74

interfacial features between the fiber and matrix is quite different. For SPC-145 (see Fig. 8a), there exists an obvious groove-like interspace, while no interspace is observed between the two for SPC-160 (see Fig. 8b). This indicates that the interfacial adhesion between iPP fiber and matrix in SPC-160 is indeed better than that in SPC-145. Hence, this can be considered as a main reason to cause the increased tensile strength of SPC-160 by 20.6% than that of SPC-145. However, for SPC-175, the boundary lines between the iPP fiber and matrix have completely disappeared. Additionally, the iPP fiber is hardly distinguished from the matrix (see Fig. 8c). It seems that SPC-175 shows the best interfacial adhesion between the iPP fiber and the iPP matrix. However, the best interfacial adhesion is at the expense of orientation relaxation due to the melting of iPP fiber, which can be confirmed by FTIR results (see Table 1). Moreover, the

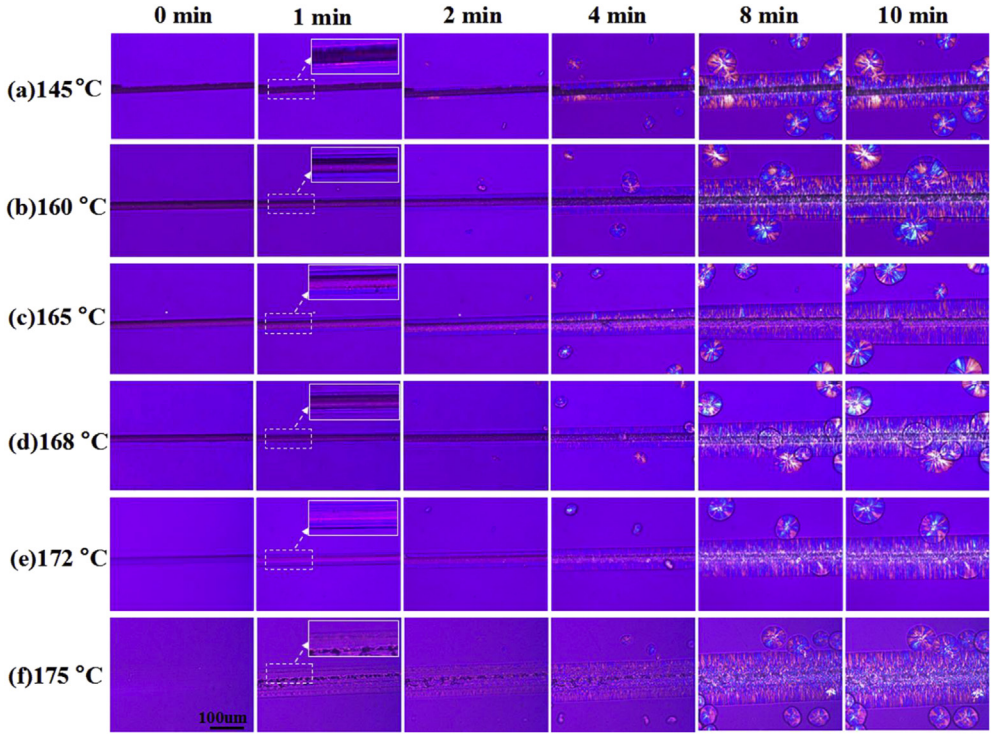

Fig. 3. Interfacial morphology evolution of SPCs prepared at different T_i during isothermal crystallization at 134 °C.

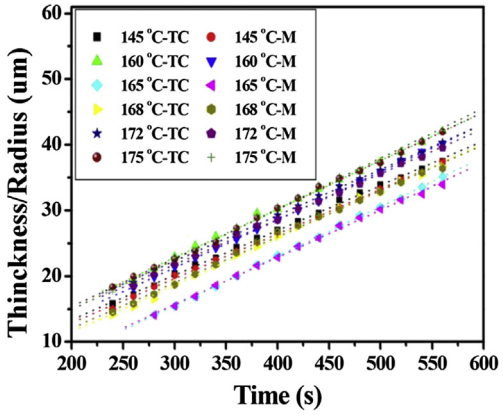

Fig. 4. The thickness of transcrystalline layer and radii of spherulites versus crystallization time in SPCs prepared at different T_i. M represents the iPP crystals in matrix.

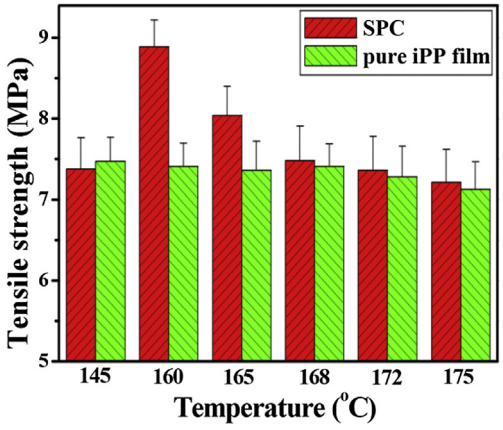

Fig. 5. Tensile strength of SPCs and pure iPP films.

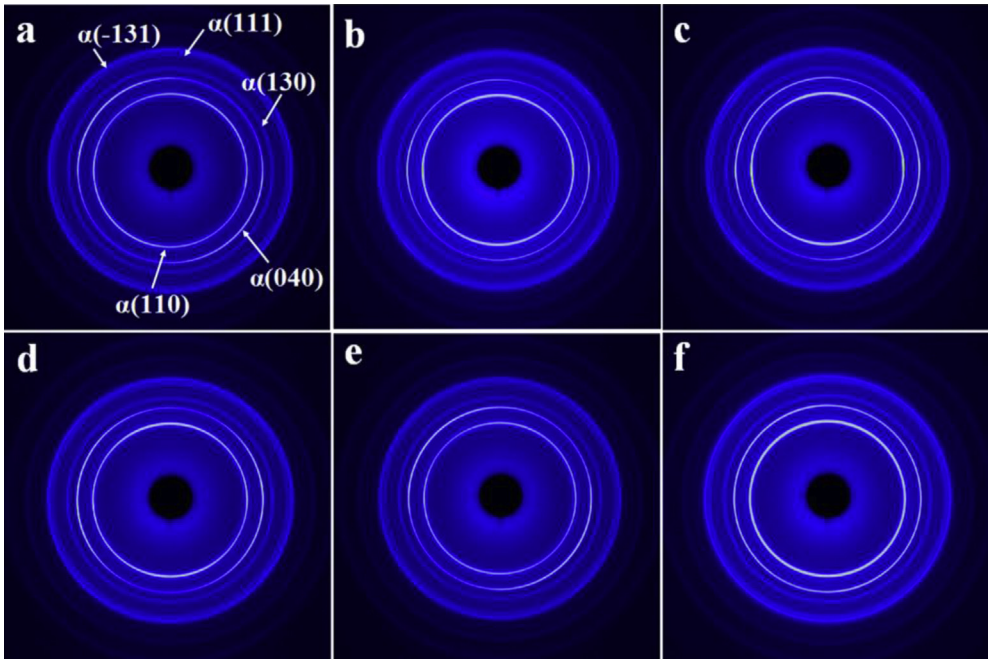

Fig. 6. 2D-WAXD patterns of SPCs prepared at different T_i: (a) 145, (b) 160, (c) 165, (d) 168C, (e) 172, and (f) 175 °C. The iPP fibers axis direction is perpendicular.

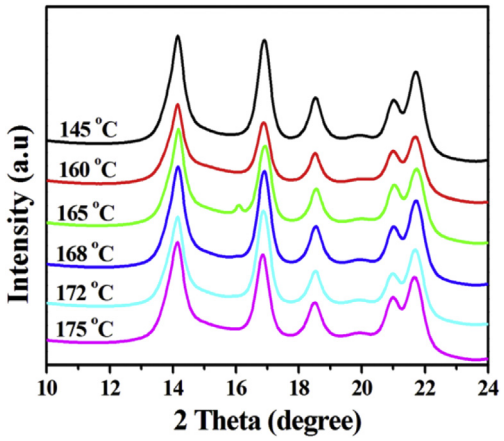

Fig. 7. 1D-WAXD curves of SPCs prepared at different T_i.

Table 2
Crystallinity of SPCs prepared at different T_i.

Samples	SPC-145	SPC-160	SPC-165	SPC-168	SPC-172	SPC-175
Crystallinity (%)	57.69	50.47	59.25	56.81	56.65	52.43

tensile strength of the iPP fiber is decreased with increasing the T_i, which is shown in Fig. S5 in Supplementary data. Therefore, it is easy to explain the decreased tensile strength of SPCs with the increase of T_i (from 165 to 175 °C).

To further understand the relationship between interfacial features and tensile strength of SPCs, Fig. 8a_1-c_1 shows the morphology of fractured zone of these respective samples (SPC-145, SPC-160 and SPC-175). As for SPC-145 (see Fig. 8a_1), one can clearly see that the fractured fiber is pulled out from the matrix (shown by the arrow), suggesting the relatively poor interfacial interaction between iPP fiber and matrix. However, with respect to SPC-160 and SPC-175 (see Fig. 8b_1 and c_1), no pull-out fiber is observed. This indicates the good interfacial interaction between iPP fiber and matrix in SPC-160 and SPC-175. More importantly, the TC around the iPP fiber was changed into the black one after the tensile test (see Fig. 8b_1 and c_1). This implies that the interfacial adhesion between fiber and matrix is so good that the stress at the interface can be transferred from the matrix to the fiber in SPC-160 and SPC-175. Therefore, combined with the orientation degree (viz., molecular orientation [43]) of the iPP fibers (see Table 1), it is easy to understand the maximum tensile strength in SPC-160. In other words, this is related to good interfacial adhesion between fiber and matrix and high tensile strength resulting from high orientation degree of iPP fiber. However, for SPC-175, good interfacial adhesion is at the expense of orientation degree of iPP fiber (verified by FTIR results shown in Table 1). Therefore, it is reasonable that tensile strength is deteriorated by further increasing the T_i.

Based on above results and discussion, three important conclusions can be drawn: (1) the iPP fiber introduced at 145 °C is almost in solid state, which can be confirmed by Fig. S1 in Supplementary data. The resultant weaker interfacial adhesion between iPP fiber and matrix leads to lower mechanical performances; (2) when T_i is elevated to 160 °C, the tensile strength of SPCs increases obviously. This is related to the surface partial melting of the iPP fiber (see DSC result shown in Fig. S1 in Supplementary data). Hence, it enhances the interfacial adhesion between the iPP fiber and matrix. Meanwhile, iPP fiber still shows high orientation degree and high tensile strength at this temperature (see Table 1 and Fig. S5 in Supplementary data). These are also the main reasons why the tensile strength of SPC-160 is higher than that of SPC-145; (3) when T_i is further increased, the tensile strength exhibits an attenuation trend. The reason is that with the increase of the T_i, an increase of interfacial adhesion between fiber and matrix is at the expense of orientation relaxation, which has been proved by the FTIR results (see Table 1). Moreover, the tensile strength of iPP fiber shows a downward trend with increasing the T_i (shown in Fig. S5 in Supplementary data). Hence, the tensile strength of SPCs decreases with increasing the T_i (from 165 to

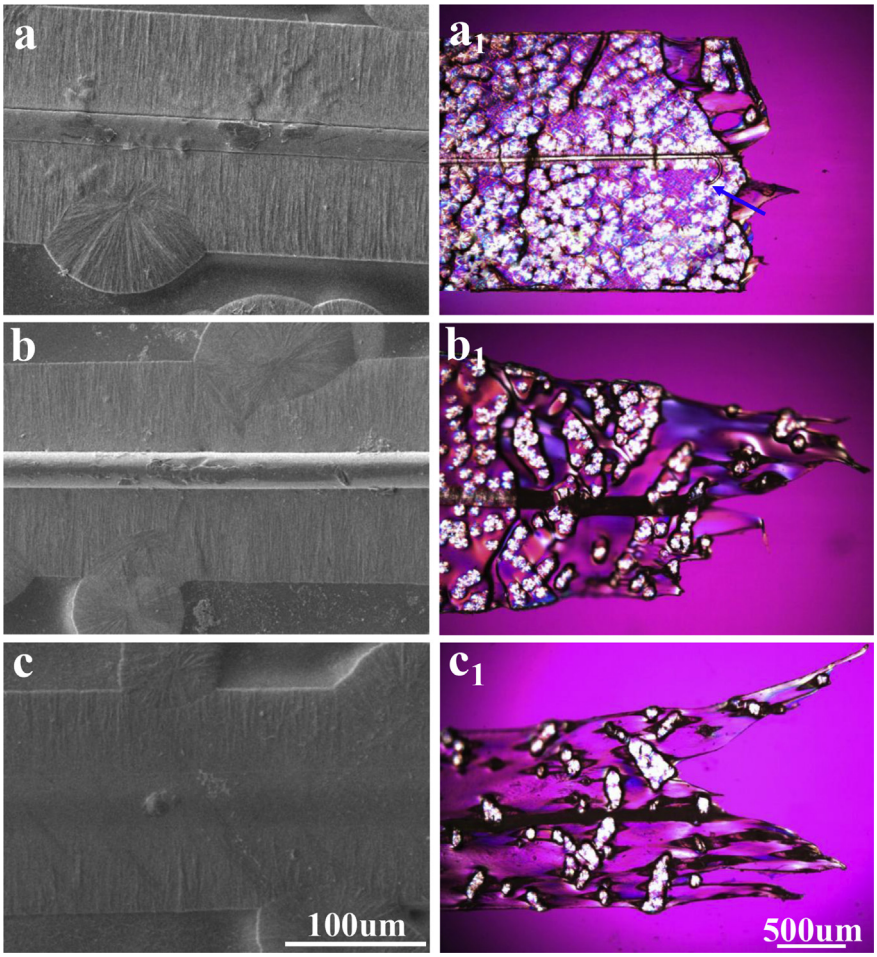

Fig. 8. (a–c) SEM images of interfacial features of SPCs, and (a_1-c_1) POM micrographs of the fractured zone of the SPCs. (a) and (a_1): SPC-145; (b) and (b_1): SPC-160; (c) and (c_1): SPC-175.

175 °C). In short, at $T_i = 160$ °C, high orientation degree and high tensile strength of iPP fiber itself, together with the good interfacial adhesion between iPP fiber and matrix are synergistically responsible for the maximum value of tensile strength.

4. Conclusions

The iPP based SPCs have been successfully prepared by introducing iPP fibers into the molten or supercooled homogeneous matrix. The induced TC by homogeneous fiber as a function of T_i was observed by means of POM. Then the relationship between interfacial features and mechanical property of SPCs was studied. The results show that the tensile strength of SPCs firstly increases and reaches a maximum value at $T_i = 160$ °C, then decreases with the increase of the T_i. Based on the detailed analysis, the mechanical enhancement of SPCs is mainly ascribed to the existence of TC, high orientation degree and high tensile strength of iPP fiber, together with good adhesion between iPP fiber and matrix. This study provides a new insight into the relationship between interfacial features and mechanical property of iPP based single-polymer composites.

Acknowledgments

We express our great thanks to the National Natural Science Foundation of China (51173171, 11172271), the Major State Basic Research Projects (2012CB025904), Plan for Scientific Innovation Talent of Henan Province and Opening Project of State Key Laboratory of Polymer Materials Engineering (Sichuan University). Z. Guo appreciates the start-up funds from University of Tennessee.

Appendix A. Supplementary data

Supplementary data related to this article can be found at http://dx.doi.org/10.1016/j.polymer.2016.02.052.

References

[1] N.M. Barkoula, T. Peijs, T. Schimanski, et al., Processing of single polymer composites using the concept of constrained fibers, Polym. Compos 26 (2005) 114–120.
[2] C. Wang, C.R. Liu, Transcrystallization of polypropylene on carbon fibres, Polymer 38 (1997) 4715–4718.
[3] G. Pompe, E. Mäder, Experimental detection of a transcrystalline interphase in glass-fibre/polypropylene composites, Compos Sci. Technol. 60 (2000) 2159–2167.
[4] J.L. Thomason, A.A. Van Rooyen, Transcrystallized interphase in thermoplastic composites, J. Mater Sci. 27 (1992) 897–907.
[5] M.A.L. Manchado, J. Blagiotti, L. Torre, J.M. Kenny, Effects of reinforcing fibers on the crystallization of polypropylene, Polym. Eng. Sci. 40 (2000) 2194–2204.
[6] N.J. Capiati, R.S. Porter, The concept of one polymer composites modelled with high density polyethylene, J. Mater Sci. 10 (1975) 1671–1677.
[7] S. Han, K. Ren, C.Z. Geng, K. Wang, Q. Zhang, F. Chen, Enhanced interfacial adhesion via interfacial crystallization between sisal fiber and isotactic polypropylene: direct evidence from single-fiber fragmentation testing, Polym. Int. 63 (2014) 646–651.
[8] S.H. Deng, X.D. Zhou, C.J. Fan, Q.F. Lin, X.G. Zhou, Release of interfacial thermal

stress and accompanying improvement of interfacial adhesion in carbon fiber reinforced epoxy resin composites: induced by diblock copolymers, Compos. Part A 43 (2012) 990–996.
[9] Z. Li, D.S. Tan, Ren Ql, Y.F. Xu, Y.F. Tao, Synthesis and properties of UV-curable polysiloxane methacrylate obtained by one-step method, Chin. J. Polym. Sci. 31 (2013) 363–370.
[10] Q.Y. Peng, X.D. He, Y.B. Li, C. Wang, R.G. Wang, P.A. Hu, et al., Chemically and uniformly grafting carbon nanotubes onto carbon fibers by poly (amido-amine) for enhancing interfacial strength in carbon fiber composites, J. Mater Chem. 22 (2012) 5928–5931.
[11] J.J. Su, G.H. Yang, C.Z. Geng, H. Deng, The variable role of clay on the crystallization behavior of DMDBS-nucleated polypropylene, Chin. J. Polym. Sci. 29 (2011) 732–740.
[12] M.S. Islam, K.L. Pickering, N.J. Foreman, Influence of alkali treatment on the interfacial and physico-mechanical properties of industrial hemp fibre reinforced polylactic acid composites, Compos. Part A 41 (2010) 596–603.
[13] L. Chen, Y.F. Xiang, K. Wang, Q. Zhang, R.N. Du, Effects of matrix molecular weight on structure and reinforcement of high density polyethylene/mica composites, Chin. J. Polym. Sci. 29 (2011) 377–389.
[14] M.A. Sawpan, K.L. Pickering, A. Fernyhough, Effect of fibre treatments on interfacial shear strength of hemp fibre reinforced polylactide and unsaturated polyester composites, Compos. Part A 42 (2011) 1189–1196.
[15] J. Karger-Kocsis, Polypropylene Structure, Blends and Composites, Springer Science and Business Media, Budapest, 1995.
[16] N.Y. Ning, S.R. Fu, W. Zhang, F. Chen, K. Wang, H. Deng, et al., Realizing the enhancement of interfacial interaction in semicrystalline polymer/filler composites via interfacial crystallization, Prog. Polym. Sci. 37 (2012) 1425–1455.
[17] I.F. Tannock, R. de Wit, W.R. Berry, J. Horti, A. Pluzanska, K.N. Chi, et al., Docetaxel plus prednisone or mitoxantrone plus prednisone for advanced prostate cancer, New Engl. J. Med. 351 (2004) 1502–1512.
[18] S.J. Zhang, M.L. Minus, L.B. Zhu, C.P. Wong, S. Kumar, Polymer transcrystallinity induced by carbon nanotubes, Polymer 49 (2008) 1356–1364.
[19] N.J. Capiati, R.S. Porter, The concept of one polymer composites modelled with high density polyethylene, J. Mater Sci. 10 (1975) 1671–1677.
[20] Á. Kmetty, T. Bárány, J. Karger-Kocsis, Self-reinforced polymeric materials: a review, Prog. Polym. Sci. 35 (2010) 1288–1310.
[21] C.C. Gao, L. Yu, H.S. Liu, L. Chen, Development of self-reinforced polymer composites, Prog. Polym. Sci. 37 (2012) 767–780.
[22] S. Fakirov, Nano-and microfibrillar single-polymer composites: a review, Macromol. Mater Eng. 298 (2013) 9–32.
[23] N.M. Barkoula, T. Peijs, T. Schimanski, J. Loos, Processing of single polymer composites using the concept of constrained fibers, Polym. Compos 26 (2005) 114–120.
[24] B. Alcock, N. Cabrera, N.M. Barkoula, T. Peijs, Low velocity impact performance of recyclable all-polypropylene composites, Compos Sci. Technol. 66 (2006) 1724–1737.
[25] T.N. Abraham, S.D. Wanjale, T. Bárány, J. Karger-Kocsis, Tensile mechanical and perforation impact behavior of all-PP composites containing random PP copolymer as matrix and stretched PP homopolymer as reinforcement: effect of β nucleation of the matrix, Compos. Part A 40 (2009) 662–668.
[26] H.H. Li, X.Q. Zhang, Y.X. Duan, D.J. Wang, L. Li, S.K. Yan, Influence of crystallization temperature on the morphologies of isotactic polypropylene single-polymer composite, Polymer 45 (2004) 8059–8065.
[27] H.H. Li, S.D. Jiang, J.J. Wang, D.J. Wang, S.K. Yan, Optical microscopic study on the morphologies of isotactic polypropylene induced by its homogeneity fibers, Macromolecules 36 (2003) 2802–2807.
[28] X.L. Sun, H.H. Li, X.Q. Zhang, D.J. Wang, J.M. Schultz, S.K. Yan, Effect of matrix molecular mass on the crystallization of β-Form isotactic polypropylene around an oriented polypropylene fiber, Macromolecules 43 (2009) 561–564.
[29] X.L. Sun, H.H. Li, X.Q. Zhang, J.J. Wang, D.J. Wang, S.K. Yan, Effect of fiber molecular weight on the interfacial morphology of iPP fiber/matrix single polymer composites, Macromolecules 39 (2006) 1087–1092.
[30] Y.J. Qin, Y.H. Xu, L.Y. Zhang, et al., Shear-induced interfacial sheath structure in isotactic polypropylene/glass fiber composites, Polymer 70 (2015) 326–335.
[31] Y.H. Song, K.H. Nitta, N. Nemoto, Molecular orientations and true stress-strain relationship in isotactic polypropylene film, Macromolecules 36 (2003) 8066–8073.
[32] Y.H. Song, K.H. Nitta, N. Nemoto, Deformation mechanisms of polymer thin films by simultaneous kinetic measurement of microscopic infrared dichroism and macroscopic stress. 2. Molecular orientation during necking process of isotactic polypropylene, Macromolecules 36 (2003) 1955–1961.
[33] G. Lamberti, V. Brucato, Real - time orientation and crystallinity measurements during the isotactic polypropylene film-casting process, J. Polym. Sci. Part B 41 (2003) 998–1008.
[34] H.H. Li, J.C. Liu, D.J. Wang, et al., A comparison study on the homogeneity and heterogeneity fiber induced crystallization of isotactic polypropylene, Colloid Polym. Sci. 281 (2003) 973–979.
[35] S.J. Zhang, M.L. Minus, L.B. Zhu, et al., Polymer transcrystallinity induced by carbon nanotubes, Polymer 49 (2008) 1356–1364.
[36] D.M. Dean, L. Rebenfeld, R.A. Register, et al., Matrix molecular orientation in fiber-reinforced polypropylene composites, J. Mater Sci. 33 (1998) 4797–4812.
[37] E. Assouline, E. Wachtel, S. Grigull, et al., Lamellar orientation in transcrystalline γ isotactic polypropylene nucleated on aramid fibers, Macromolecules 35 (2002) 403–409.
[38] G. Natta, P. Corrasini, Nuovo Cimento Supplemento15, 1960, pp. 40–51.
[39] A. Turner-Jones, A.J. Cobbold, The β crystalline form of isotactic polypropylene, J. Polym. Sci. Part B 6 (1968) 539–546.
[40] M. Zhou, Y.H. Li, C. He, T.X. Jin, K. Wang, Q. Fu, Interfacial crystallization enhanced interfacial interaction of poly (butylene succinate)/ramie fiber biocomposites using dopamine as a modifier, Compos Sci. Technol. 91 (2014) 22–29.
[41] X.F. Zhao, R.K.Y. Li, S.L. Bai, Mechanical properties of sisal fiber reinforced high density polyethylene composites: effect of fiber content, interfacial compatibilization, and manufacturing process, Compos. Part A 65 (2014) 169–174.
[42] C.M. Wu, M. Chen, J. Karger-Kocsis, Effect of micromorphologic features on the interfacial strength of iPP/Kevlar fiber microcomposites, Polymer 42 (2001) 199–208.
[43] D. Campbell, M.M. Qayyum, Enhanced fracture strain of polypropylene by incorporation of thermoplastic fibres, J. Mater Sci. 12 (1997) 2427–2434.